APL Materials

MoS_2 for beyond lithium-ion batteries

Cite as: APL Mater. **9**, 050903 (2021); https://doi.org/10.1063/5.0050118
Submitted: 12 March 2021 • Accepted: 05 May 2021 • Published Online: 17 May 2021

Feipeng Yang, Xuefei Feng, Per-Anders Glans, et al.

MoS_2 for beyond lithium-ion batteries

Cite as: APL Mater. 9, 050903 (2021); doi: 10.1063/5.0050118
Submitted: 12 March 2021 • Accepted: 5 May 2021 •
Published Online: 17 May 2021

Feipeng Yang,[1,2] Xuefei Feng,[1,2] Per-Anders Glans,[2] and Jinghua Guo[1,2,3,a)]

AFFILIATIONS

[1] Joint Center for Energy Storage Research, Lemont, Illinois 60439, USA
[2] Advanced Light Source, Lawrence Berkeley National Laboratory, Berkeley, California 94720, USA
[3] Department of Chemistry and Biochemistry, University of California Santa Cruz, Santa Cruz, California 95064, USA

[a)] **Author to whom correspondence should be addressed:** jguo@lbl.gov

ABSTRACT

As a typical transition-metal chalcogenide material, molybdenum disulfide (MoS_2) has received tremendous attention because of its unique layered structure and versatile chemical, electronic, and optical properties. With the focus of this Perspective on the energy storage area, one of the most important contributions of MoS_2 is that it sparked the birth of the rechargeable lithium battery in the early 1980s, which later formed the foundation of commercial lithium batteries. After four decades, admitting that MoS_2 is still playing a significant role in the lithium-ion battery field and considerable effort was made to decipher the mechanism through *ex situ* and *in situ* studies and by means of MoS_2 nanostructure engineering that advances the lithium battery performance, it is also used in beyond lithium-ion batteries, such as sodium, magnesium, calcium, and aluminum energy storage systems. Such alternative battery systems are desirable because of the safety concerns of lithium and the depletion of lithium reserves and corresponding increase in cost. In this Perspective, recent development on the fabrication of novel MoS_2 nanostructures was discussed, followed by the scrutinization of their application in beyond lithium-ion batteries and the *in situ*/*operando* methods involved in these studies. Finally, a brief summary and outlook that may help with the future advancement of the beyond lithium-ion batteries are presented.

I. INTRODUCTION

Efficient and economical energy storage is becoming significant because of the threat from global climate change, growing demand for energy, and depletion of fossil fuel reserves.[1,2] The lithium-ion battery has been quite successful commercially because of its high energy density, lightweight, wide operating voltage, and high efficiency.[3,4] The research on the lithium battery started more than forty years ago, when the group VI layered disulfides were not of interest for most scientists because of their poor rechargeability.[5] Nevertheless, it was discovered that in molybdenite, the natural form of molybdenum disulfide (MoS_2), when the Mo coordination is changed from trigonal prismatic to octahedral, MoS_2 can be used as an electrode effectively. This system from Haering *et al.* sparked the foundation of a commercial battery.[5] Since then, MoS_2 has attracted substantial attention and was investigated comprehensively as an electrochemical storage material,[6,7] catalyst,[8–11] and solid lubricant.[12–14]

MoS_2 as a typical transition-metal sulfide has a two-dimensional, layered S–Mo–S stacking structure and numerous active sulfur sites that offer numerous advantages for electrochemical energy storage.[15–17] Each of the Mo atoms in MoS_2 stacking layers is coordinated by six S atoms.[18] In the layers stacked together, covalent bonds connect atoms within the MoS_2 layer, while van der Waals interactions bond together the individual layers.[19,20] The interlayer distance in MoS_2 is ~0.62 nm, compared to the 0.34 nm spacing in graphite; this larger spacing between the S layers bestows fast diffusion of lithium without volume expansion.[17] As a reversible intercalation host, it is considered as a desirable anode material for secondary batteries,[21,22] such as that used in lithium-ion batteries.[23,24] The theoretical capacity for MoS_2 through a complete conversion reaction, $MoS_2 + 4Li^+ + 4e^- \rightarrow 2Li_2S + Mo$, is 669 mA h/g.[25–27] This mechanism is comparable to the pioneering work by Jacobson *et al.* with respect to the electrochemical properties of amorphous Li/MoS_2.[28] However, the MoS_2 electrodes can provide a higher value of 1100 mA h/g at 0.5 A/g with an excellent retention rate, reversibility, and cyclic stability.[29] In recent years, advancement in the electrochemical performance of MoS_2 has been improved through the precise design and control of the nanosize and morphology,[30–34] and there are many reported charge storage

capacities for the MoS_2 nanostructures higher than the MoS_2 theoretical value.[35,36] The reaction mechanism for the lithium intercalation in MoS_2 anodes is still under investigation despite decades of effort.[16] One possible hypothesis is that the alkali sulfides will be oxidized and will generate S atoms, while the Mo atoms will remain inert electrochemically.[37,38] Another assumption is that the extra capacity results from the formation of a space charge layer with Li^+ at the metal/lithium electrolyte interface, while the charge is counteracted by the electrons on the metal surface.[39]

In situ/*operando* characterization methods, especially those sensitive to the electrode/electrolyte interface, have received more attention and been involved in scrutinizing the mechanism under working conditions.[17,32] For example, *in situ*/*operando* soft x-ray absorption spectroscopy (XAS) enables probing of such an electrode/electrolyte interface while an electrochemical bias is applied, shedding light on the facile solvation and desolvation at an electrified interface, which is critical for continuous operations. A comparison between the total electron yield (TEY) and total fluorescence yield (TFY) detection modes also indicates that the interface between the liquid electrolyte and the solid electrode can be different from the bulk when the electrochemical bias is applied.[40] The details of using such *operando* XAS in the probing of MoS_2 anode intercalation and conversion reactions at the interface in lithium-ion cells will be discussed in Sec. IV.

As a consequence of safety issues caused by dendrite formation, the depletion of lithium reserves, and the corresponding cost increase, an alternative energy storage system with large storage capacity and stability becomes growingly desirable.[4] Additionally, considering the global climate change, the utilization of renewable energies, such as solar and wind power, requires efficient energy storage that levels their intermittent output, making it possible to integrate to the electric grid. The lithium-ion battery in this case is not the best candidate for large-scale electrochemical energy storage applications.[1,41,42] The beyond lithium-ion batteries such as Na-ion, Mg-ion, Zn-ion, and Ca-ion batteries are lower in terms of cost because of their higher abundance in nature while suffering from moderate energy density, low capacity, low cell voltage, and low energy density, respectively.[43] Meanwhile, Na-ion batteries are cost-efficient, sustainable, and safe; Mg-ion batteries are high in capacity, dendrite-free, and sustainable; Ca-ion batteries are similar in volumetric capacity compared to that of Li-ion batteries; and Zn-ion batteries offer potential in grid-scale related energy storage.[43–45] Starting from Sec. II, the use of MoS_2 in the Na-ion, Mg-ion, Zn-ion, Ca-ion, and Al-ion batteries will be briefly reviewed. Additional relevant applications of MoS_2 such as in the catalysis including hydrogen evolution, nitrogen reduction, and CO_2 reduction will be introduced. In Sec. IV, the experimental approaches involved in these studies with an emphasis on the use of *in situ* and *operando* characterization techniques will be presented. Finally, a brief summary of the MoS_2 in the advancing of beyond lithium-ion batteries and our opinion on the future prospects will be discussed.

II. FABRICATION AND NANOSTRUCTURE ENGINEERING

MoS_2 has been studied extensively because of its wide applications, such as those in the electrochemical energy storage, and optical properties.[2,46] For a two-dimensional transition-metal dichalcogenide, various approaches have been used in the fabrication of the atomically thin film consisting of one Mo layer and two S layers (S–Mo–S). As shown in Fig. 1, typical fabrication methods include a top-down method by mechanical exfoliation,[47] high-energy sonication,[2] and a bottom-up approach through chemical vapor deposition (CVD), and wet-chemical synthesis, including hydrothermal and solvothermal methods. A typical top-down method starts from bulk MoS_2 powder, and exfoliation can be performed using mechanical force, e.g., the Scotch-tape method, which produces highest-quality monolayered samples, or using liquid, which is suitable for fundamental demonstrations in applications in which a large amount of materials are necessary.[47–49] Typical solvents used in the liquid sonication exfoliation are N-methyl-2-pyrrolidone and dimethylformamide.[50,51] The bottom-up approach, CVD, has been considered as a breakthrough that enabled the preparation of large area MoS_2 layers.[52,53] It involves a two-step thermolysis during which a dip-coating process in ammonium thiomolybdates $[(NH_4)_2MoS_4]$ follows by annealing at 500 °C and sulfurization at 1000 °C in sulfur vapor.[53] During the thermolysis, MoS_2 layers formed through the reaction of $(NH_4)_2MoS_4 + H_2 \rightarrow 2NH_3 + 2H_2S + MoS_2$. Wet chemistry is another bottom-up approach generally used in the fabrication of MoS_2 layers, including solvothermal and hydrothermal methods. Schematics of using $(NH_4)_6Mo_7O_{24}{\cdot}4H_2O$ + thiourea via the solvothermal method and $Na_2MoO_4{\cdot}2H_2O + NH_2CSNH_2$ via the hydrothermal method are shown in Figs. 1(2c) and 1(2d), respectively. The different MoS_2 phases can be obtained by annealing at different temperatures, e.g., 1050 °C in an Ar atmosphere for 1T-phase and 400 °C for 2H-phase MoS_2 from hydrothermal fabrication.[54]

In addition to the traditional methods mentioned above, in recent years, a novel atomic layer deposition (ALD) process as a precisely controlled bottom-up approach has also been developed and used in the fabrication of the MoS_2 film.[46] As one of the most rapidly developing thin film fabrication techniques, the ALD fabrication process can be precisely controlled because of its self-controlled mechanism in which the alternating growth of the film is dictated by two self-limiting gas–solid surface reactions.[58] Additionally, ALD produces conformal films, making it one of the very few techniques suitable for semiconductor industry where miniaturization is critical, even on very high aspect structures.[59] As shown in the schematic of ALD in Fig. 2(a), the ALD process generally involves binary reaction sequences during which two surface reactions take place and they are intrinsically self-limiting, which allows the two reactions to proceed sequentially to fabricate a thin film with atomic or monolayer level control. Although part of the surface will react with the precursor gas before some other parts, especially for some high aspect ratio surfaces, the precursors will also first desorb from the surface areas where the reaction is completed and proceed to react with other unreacted parts, making conformal deposition. For the ALD growth of MoS_2, binary reaction sequences occur through alternating exposure to molybdenum chloride ($MoCl_5$) and hydrogen disulphide (H_2S).[46] As shown in Fig. 2(b), one growth cycle starts with exposure to $MoCl_5$, dwelling, N_2 purge, H_2S exposure, dwelling, and N_2 purge. The reported reaction temperature for this ALD was 300 °C, and post-annealing at 800 °C was used to improve crystallinity. Faceted triangular crystals will be formed by the reconstruction of the as-deposited MoS_2 thin film on the sapphire. A

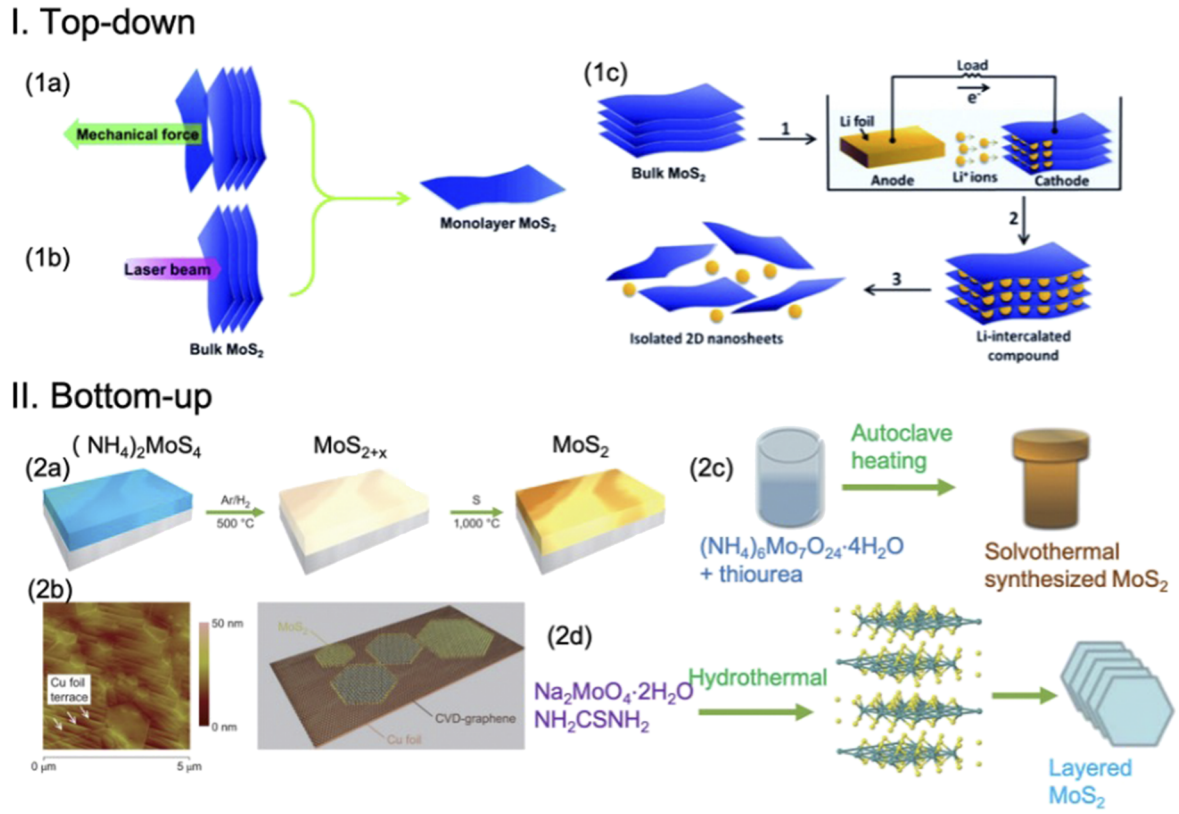

FIG. 1. Fabrication of MoS_2 methods. (I) Top-down approaches to prepare the MoS_2 nanosheets via (1a) mechanical exfoliation, (1b) laser exfoliation, and (1c) electrochemical intercalation exfoliation methods. (II) Bottom-up preparation methods including the schematic of (2a) the MoS_2 layer deposited by two-step thermolysis, (2b) MoS_2 nanosheets on CVD graphene/Cu foil, and (2c) and (2d) solvothermal and hydrothermal fabrication of MoS_2 layered structures. Reproduced with permission from Wang *et al.*, Adv. Sci. **4**, 1600289 (2017). Copyright 2017 Wiley-VCH Verlag GmbH & Co. KGaA, Weinheim;[2] reproduced with permission from Chhowalla *et al.*, Nat. Chem. **5**, 263 (2013). Copyright 2013 Nature Publishing Group;[47] reproduced with permission from Zeng *et al.*, Angew. Chem., Int. Ed. **50**, 011093 (2011). Copyright 2011 Wiley-VCH Verlag GmbH & Co. KGaA, Weinheim;[55] reproduced with permission from Zhang *et al.*, Nanoscale **7**, 018364 (2015). Copyright 2015 Royal Society of Chemistry;[56] and reproduced with permission from Liu *et al.*, Nanoscale **5**, 9562 (2013). Copyright 2013 Royal Society of Chemistry.[57]

cross-sectional transmission electron microscopy (TEM) image of the MoS_2 film in Fig. 2(c) shows that the interlayer spacing is 0.610 nm for the (002) planes. For 10 and 50 ALD cycles, the film thickness values are ~1.5 and 9 nm, respectively.

MoS_2 of different geometrical structures and on different supporting substrates are being reported to promote their performance in catalysis and battery systems, including MoS_2 microspheres,[60,61] fullerene-like nanoparticles,[21] MoS_2 supported by graphene sheets or reduced graphene oxide (rGO),[19,57] and MoS_2-PEO and other MoS_2 composites.[20,62,63] For example, in the fabrication of Mg batteries, the triple layered structure of MoS_2 makes it convenient for insertion and extraction of Mg^{2+} ions. The morphologies and nanostructures of MoS_2 have significant effects on the electrochemical properties of the electrode materials.[64] The formation of the sandwich-structured graphene-like MoS_2/C microspheres reported by Liu *et al.* is shown in Fig. 3(a), where the MoS_2 nanosheets were fabricated by a Na_2MoO_4 and NH_2CSNH_2 hydrothermal reaction.[61] Glucose was added to the solution, during which it was dehydrated and polymerized to form oligosaccharides. Finally, intermolecular dehydration occurred between oligosaccharides, and then colloidal carbonaceous spheres formed through cross-linking and carbonization. Such a synthesis makes the MoS_2 nanosheets well dispersed in the colloidal carbonaceous spheres, and the carbonaceous materials also prevent MoS_2 from stacking together. The electrochemical performance was improved as a result of the better electronic conductivity of MoS_2 by carbon coating, the better accessibility for electrolyte because of the graphene-like structure, and the enhancement of Mg^{2+} insertion kinetics due to the enlarged interplanar spacing of MoS_2. In a separate work on rechargeable aluminum-ion batteries, MoS_2 microspheres were fabricated also using a hydrothermal method using $(NH_4)_6Mo_7O_{24}{\cdot}4H_2O$ as the Mo-source and $(NH_2)_2CS$ as the S source.[60] A schematic of the hydrothermal process and SEM of the microspheres as-prepared are shown in Fig. 3(b). The battery system based on the MoS_2 microsphere cathode, ionic liquid electrolyte, and metal aluminum anode exhibits excellent electrochemical performance as a consequence of the Al^{3+} insertion and phase transformation in the electrode material. In another work, a novel hollow-cage fullerene-like nanoparticle was synthesized through the hydrothermal method at 180 °C using Na_2MoO_4 and a sulfurization reagent CH_3CHNH_2 under a

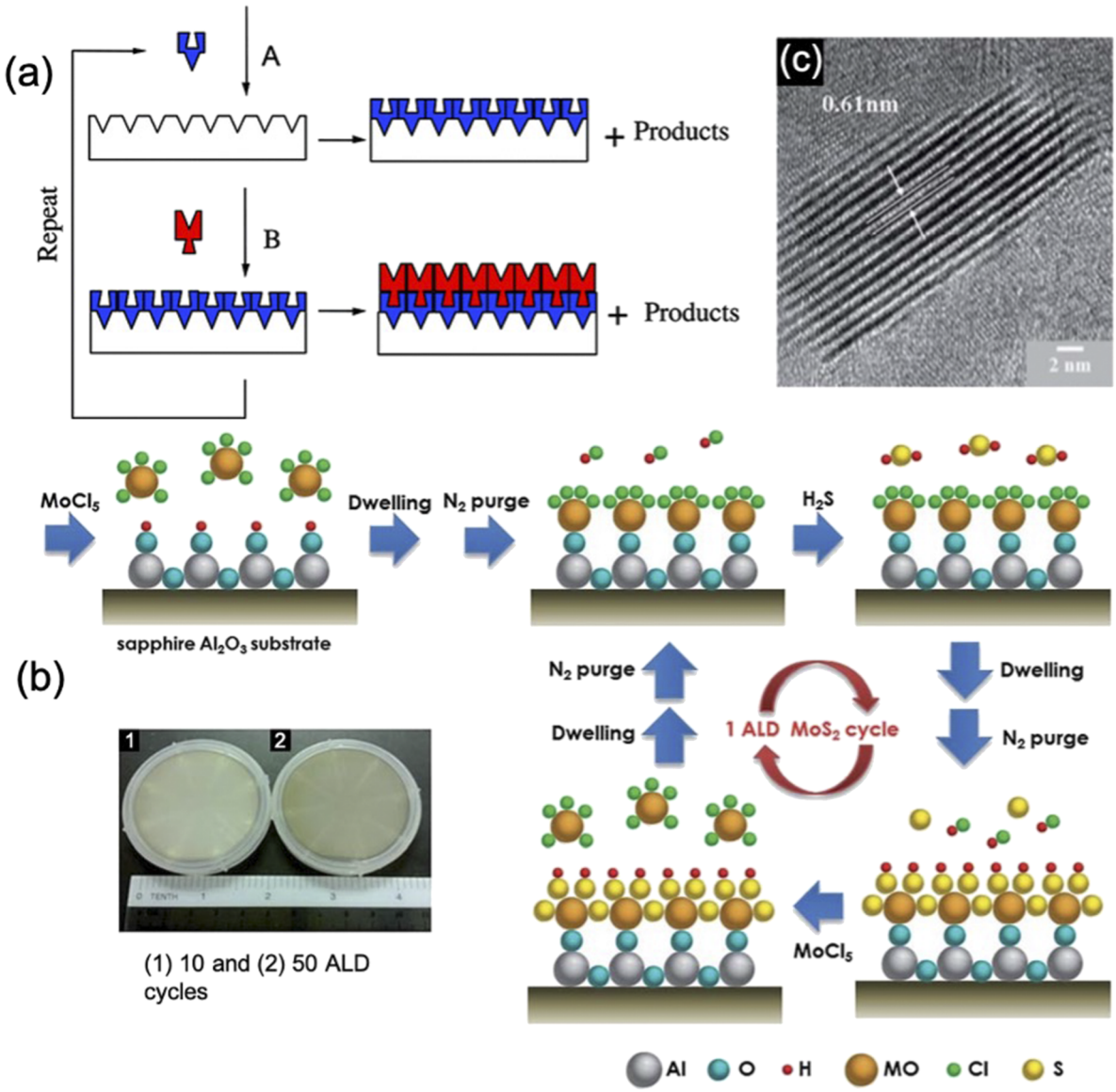

FIG. 2. (a) A schematic of ALD using self-limiting surface chemistry and AB binary reaction sequence. (b) Schematic illustration of the ALD growth cycle of the MoS_2 film and photos of (1) 10 and (2) 50 cycles of the ALD MoS_2 film. (c) Lattice spacing from a cross-sectional TEM. Reproduced with permission from Tan *et al.*, Nanoscale **6**, 10584 (2014). Copyright 2014 Royal Society of Chemistry[46] and reproduced with permission from George, Chem. Rev. **110**, 111 (2010). Copyright 2010 American Chemistry Society.[59]

pH < 1 acidic environment.[21] As shown in Fig. 3(c), the TEM images of MoS_2 nanoparticles exhibit a polygonal shape with a diameter of around 150 nm. Such fullerene-like nanoparticles prepared have a relatively large amount of broken tips, which makes them suitable for ion intercalation.

MoS_2 was also fabricated on supporting materials such as graphene or rGO to form hybrids.[19,57] Typically, $Na_2MoO_4{\cdot}2H_2O$, NH_2CSNH_2, and different amounts of GO were used in the hydrothermal process under acidic conditions (pH = 6.5) at 210 °C. The hybrids interlace between the MoS_2 and the rGO nanosheets to form sandwich-like MoS_2/rGO microspheres [Fig. 3(d)]. The stacking of MoS_2 was significantly inhibited by the supporting rGO, therefore providing favorable contribution to the rechargeable Mg batteries, e.g., higher discharge capacity and superior cycling performance. In the research of beyond lithium-ion batteries, one critical issue is to develop new intercalation hosts with different interlayer spacings to facilitate the diffusion of cations, and composites were involved in expanding such an interlayer to accommodate a Na ion with a radius of 1.06 Å compared to that of a lithium ion with a radius of 0.76 Å. As shown in

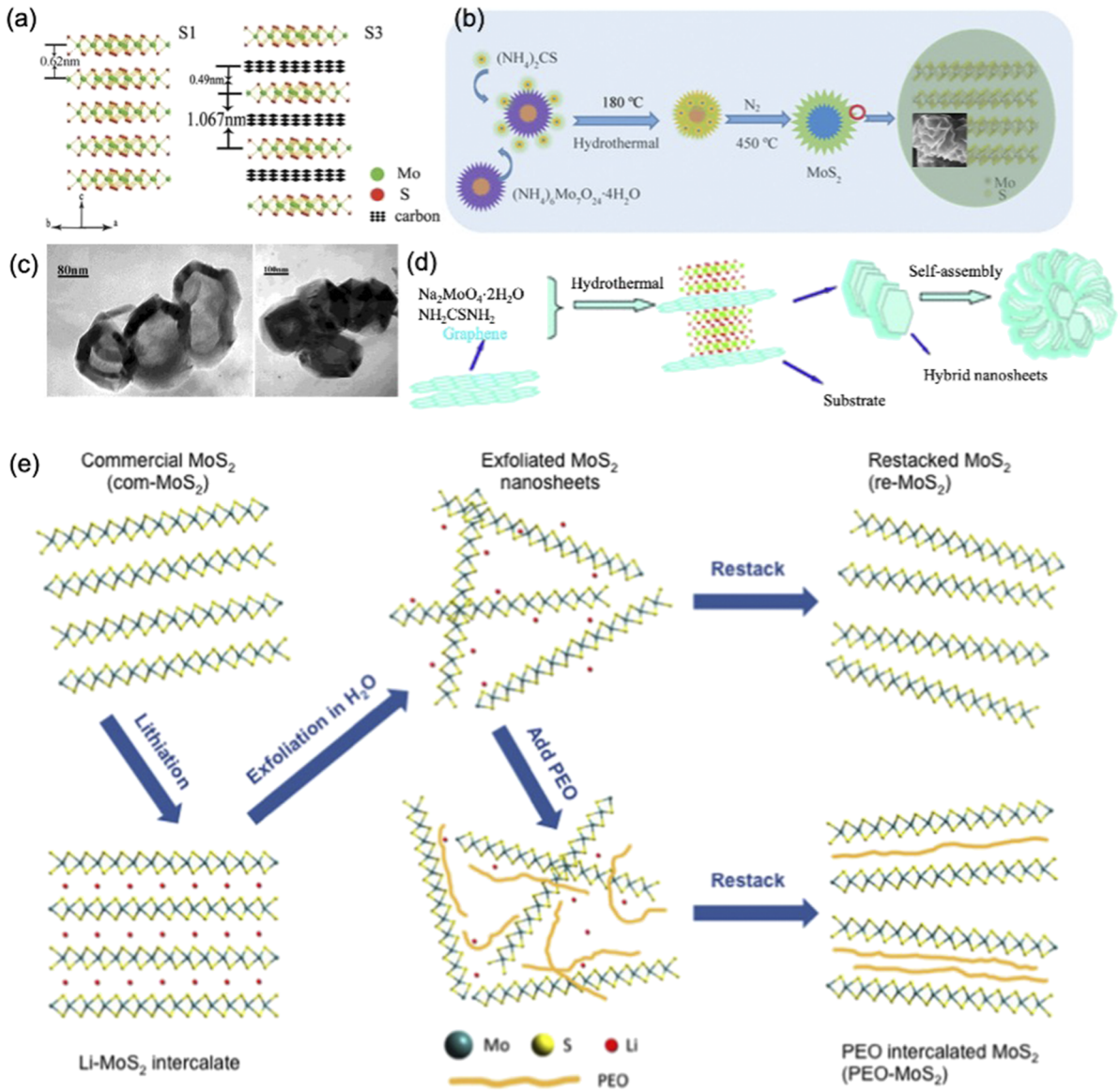

FIG. 3. (a) A schematic illustration of the microstructures of MoS_2 and a MoS_2/C composite. (b) A schematic of the hydrothermal process for MoS_2 microsphere formation and a SEM image of the MoS_2 microsphere. (c) TEM images of MoS_2 fullerene-like nanoparticles. (d) A schematic formation of the sandwich-structured MoS_2/rGO microspheres. (e) A schematic diagram of the formation of restacked MoS_2 and PEO-MoS_2 by exfoliation-restacking. Reproduced with permission from Li and Li, J. Phys. Chem. B **108**, 013893 (2004). Copyright 2004 American Chemistry Society;[21] reproduced with permission from Liu *et al.*, Nanoscale **5**, 9562 (2013). Copyright 2013 Royal Society of Chemistry;[57] reproduced with permission from Li *et al.*, ACS Appl. Mater. Interfaces **10**, 9451 (2018). Copyright 2018 American Chemistry Society;[60] reproduced with permission from Liu *et al.*, J. Mater. Chem. A **1**, 5822 (2013). Copyright 2013 Royal Society of Chemistry;[61] and reproduced with permission from Li *et al.*, Nano Energy **15**, 453 (2015). Copyright 2015 Elsevier Ltd.[62]

Fig. 3(e), poly(ethylene oxide)-intercalated MoS_2 (PEO-MoS_2) composites were fabricated through an exfoliation-restacking method for sodium-ion batteries.[62] The preparation of the restacked MoS_2 starts with commercially available MoS_2 and reaction with *n*-butyllithium in a Schlenk flask. After stirring overnight, the mixture was filtrated and washed with hexane and dried under vacuum to form $LiMoS_2$. The MoS_2 colloid will form through mixing of $LiMoS_2$ with deionized water and sonication. Composites can be fabricated by mixing the PEO aqueous solution with the MoS_2 colloid. PEO is cation-conducting and expands the lattice up to 160%, making the specific capacity more than twice that of the common MoS_2 under a current density of 50 mA/g as well as improving the cycling stability in sodium-ion batteries. Such a synthesis and strategy can also be applied to other host materials to provide high performance

electrode materials for the storage of larger cations compared to lithium.

III. MoS_2 IN BATTERY APPLICATIONS

A. MoS_2 in monovalent batteries

Efficient and economical energy storage is becoming significant because of the increasing electric vehicles and portable electronic devices. Among all the candidates, the lithium-ion battery is considered as the most promising energy storage device in portable applications.[4,65] As an anode material, the two dimensional MoS_2 exhibits a stable cycling stability and a high capacity of 1290 mA h/g,[66] benefiting from its large specific surface area and abundant voids or defects, which provide better lithium-ion diffusion pathway during the charging and discharging process.[67] The two dimensional MoS_2 reacts with the lithium-ion according to the conversion reaction of $MoS_2 + 4Li^+ + 4e^- \rightarrow Mo + 2Li_2S$ with a theoretical capacity of 670 mA h/g.[68] The MoS_2 anodes still suffer from capacity fading and poor rate behavior because of their intrinsic low electronic conductivity and aggregation during cycling. A strategy to avoid this issue is using nanostructure engineering to build structures that are difficult to restack and hybrid with carbon materials to enhance the electron transport and promote the structural stability.[31,69] An example of a hierarchical porous MoS_2/C flower-like microsphere is shown in Figs. 4(a)–4(c), which is fabricated using a solvothermal method. The flower-like microsphere structure and

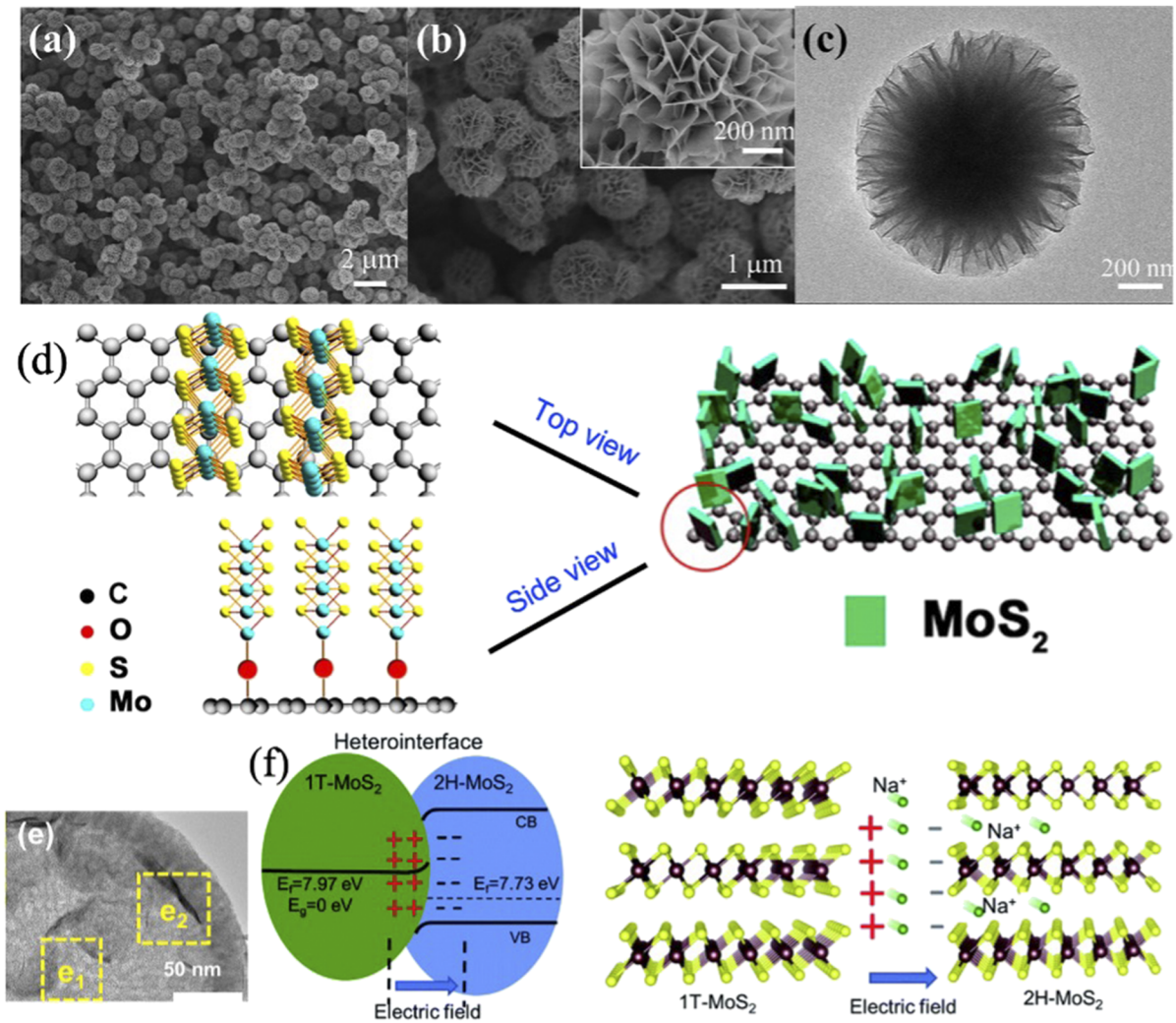

FIG. 4. (a) and (b) SEM images and (c) TEM image of the MoS_2/C microspheres. (d) A schematic of the MoS_2/G. (e) High resolution TEM image of the MoS_2 yolk–shell nanosphere. (f) A schematic of the formation mechanism and intrinsic electric field at the 1T-/2H-heterointerface. Reproduced with permission from Teng *et al.*, ACS Nano **10**, 8526 (2016). Copyright 2016 American Chemical Society;[19] reproduced with permission from Xiong *et al.*, J. Alloys Compd. **673**, 215 (2016). Copyright 2016 Elsevier Ltd.;[69] reproduced with permission from Hou *et al.*, Nano Energy **62**, 299 (2019). Copyright 2019 Elsevier Ltd.;[75] and reproduced with permission from Wu *et al.*, J. Mater. Chem. A **8**, 2114 (2020).[76]

carbon coating introduced a high interfacial contact area between the anode and the electrolyte, which favors the electron and lithium-ion transportation and prevents the active anode material aggregation. Used as an anode material in the lithium-ion battery, such a MoS_2/C flower-like microsphere provides a high specific capacity of 1125.9 mA h/g, good cycling stability, and enhanced rate performance.[69] Building hybrid nanostructures using graphene and rGO was also introduced to prevent the MoS_2-based anodes from rapid capacity fading.[19,70,71] Graphene stands out from the various kinds of carbon based materials because of its exceptional properties such as high electrical conductivity, excellent mechanical properties, thermodynamic stability, and a large specific surface area.[68,72] In a meticulously designed nanostructure with MoS_2 nanosheets [Fig. 4(d)] grown vertically on graphene sheets (MoS_2/G), the coupling of edge Mo of MoS_2 with the oxygen from GO functional groups (C–O–Mo bonds) is proposed.[19] The graphene sheets disperse the active MoS_2 and improve the electrical conductivity of the composite. The interfacial interaction of the C–O–Mo bonds also increases the structural stability and electron transport. As an anode material for lithium-ion batteries, the MoS_2/G electrode exhibits excellent cycling life and rate capability. In a similar work using rGO, by employing the MoS_2/rGO composite as the anode and activated carbon as the cathode, the hybrid lithium-ion capacitor exhibits an ultrahigh specific energy density and long cycling stability.[70] The exfoliated MoS_2 has also been used in the all-solid-state lithium-ion batteries, in which it exhibited a high discharge capacity of 439 mA h/g.[3] The mechanism of the consistently reported reversible charge storage capacities of MoS_2 higher than the theoretical value (670 mA h/g) has been investigated using TEM, Raman, and x-ray photoelectron spectroscopy (XPS) in a confined graphene nanoreactor.[16] The contribution to the extra capacity in the system is attributed to the generation of Mo atoms and subsequent reversible reaction with lithium ions, producing Mo/Li_x. The atomically dispersed Mo precipitates in the Li_2S matrix, accommodating a large number of lithium ions. The reversible Mo → Li_xMo → Mo → 1T-MoS_2 reaction cycle was the critical foundation for the superior cycling stability and capacity.

Although the lightweight, wide operating voltage, and good efficiency dominate in the portable electronics, the safety concerns, depletion of lithium reserves, and corresponding cost increase have promoted the development of sodium-ion batteries as an alternative to lithium-ion batteries. The charge–discharge mechanism of Na/MoS_2 is a two-step process: the first step is xNa + MoS_2 → Na_xMoS_2 ($x \leq 0.5$) and then the second step is 0.51Na + Na_xMoS_2 → Na_yMoS_2 ($0.5 \leq y < 1.1$).[73] The MoS_2 structure does not change during the first step but distorts in the second one. Several stable and metastable intermediate phases in the sodium intercalation were identified, including $Na_{0.375}MoS_2$, $Na_{0.625}MoS_2$, $Na_{0.75}MoS_2$, $Na_{1.0}MoS_2$, and $Na_{1.75}MoS_2$. A phase transformation from 2H- to 1T-MoS_2 and the sodium ion ordering were confirmed when the sodium content was 0.375.[74] When forming a composite with carbon materials, a sodium ion battery with a high capacity of 400 mA h/g at 0.25 C and long cycling stability was achieved.[63] MoS_2 in confined yolk–shell nanospheres were also designed and fabricated, and as shown in the TEM in Fig. 4(e), the hollow mesoporous carbon nanospheres can effectively prohibit physical detachment or loss of active materials during the sodiation and desodiation process.[75] The coexistence of both the 1T- and 2H-phases can also promote the electrical conductivity and sodium ion diffusivity compared to the 2H-MoS_2 because of the expanded interlayer spacing.[76] The electrostatic potential built intrinsically between the 1T and 2H-phases can also attract the sodium ion to the 2H-MoS_2 part, thus promoting its migration, as shown in Fig. 4(f).

The dual-ion batteries also attracted significant attention due to their high energy density, environmental friendliness, and low cost.[77] Nanostructure engineering of the MoS_2/carbon composites is investigated for dual-ion storage for their applications as batteries and pseudocapacitors.[34,77] The first-principles calculations also showed that the strain can significantly increase the adsorption energy and narrow the n-doped semiconducting gap of MoS_2, which enhances the stability, implicating the promise of applying mechanical strain on the energy storage applications.[78]

To briefly summarize the effort in lithium and sodium ion batteries, the interlayer structure engineering is critical and the introduction of carbonous material to form composites will remarkably enhance the lithium-ion storage. MoS_2 nanocomposites with different nanostructures can be a new opportunity for future design of energy storage devices involving MoS_2 anodes. The *in situ*/*operando* testing methods to tackle the evolution of the oxidation state and coordination environment and to probe interfacial structures, especially such buried interfaces, may be of great interest to employ and to further develop.[4,79]

B. MoS_2 in multivalent batteries

Multivalent batteries are promising candidates for the post-lithium-ion batteries in the development of cost-effective new energy storage. The higher theoretical volumetric capacity of the multivalent metal anode and restricted dendrite formation are the primary advantages of such post-lithium-ion multivalent batteries.[80] A significant amount of work in this area is focused on magnesium (Mg) because of its high theoretical specific capacity (2205 mA h/g and 3833 mA h/cm^3) and relatively low electrode potential [−2.36 V vs standard hydrogen electrode (SHE)], material abundance, operational safety, and environmental friendliness.[81] Early in 2004, novel structures of MoS_2, including fibrous floccus, spherical nanovesicles, platelets, nanorods, and hollow-cate fullerene-like particles, were synthesized through solution chemical reactions of Na_2MoO_4 and sulfurization reagents such as CH_3CSNH_2. Such precisely designed nanostructures provide better reversible intercalation/deintercalation cycles for Mg^{2+} ions.[21] Using a similar approach as that used in the MoS_2 fabrication for lithium and sodium batteries, phase transformation from 2H to 1T of the microscale MoS_2 makes it capable of reversibly storing Mg^{2+} and Mg^{2+}/Li^+ in all-phenyl-complex electrolytes and with a high capacity (225 mA h/g) and long cycling stability.[1] MoS_2/C composites with different geometries such as sandwich-like or graphene-like have also been synthesized through hydrothermal and solvothermal routes, respectively.[61,64] As shown in Figs. 5(a) and 5(b), combining the graphene-like MoS_2 and ultrasmall Mg nanoparticles with an average diameter of 2.5 nm, a high operating voltage (1.8 V), a high discharge capacity (170 mA h/g), and long cycling stability was achieved. The reactions in this magnesium ion battery can be confirmed as $6MoS_2 + 4Mg \rightarrow Mg_4Mo_6S_{12}$. The sandwich-structured graphene-like MoS_2/C microspheres make the composite accessible for the electrolyte, expediting the transportation of Mg^{2+}

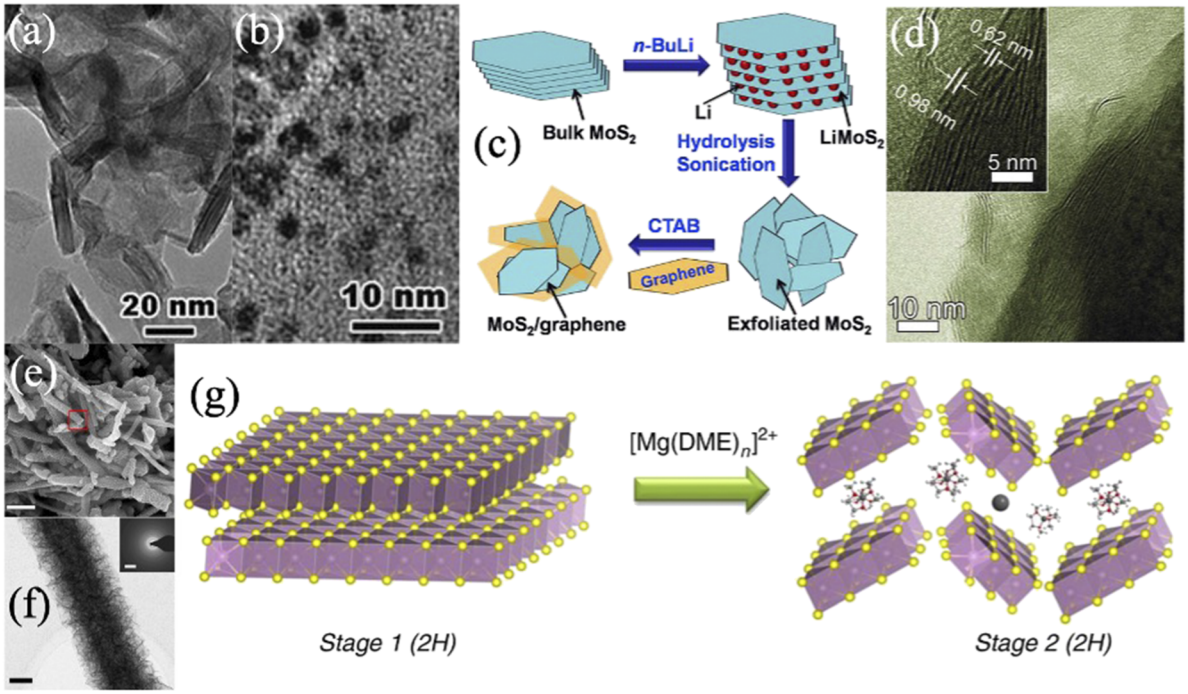

FIG. 5. TEM image of (a) graphene-like MoS_2 and (b) Mg nanoparticles. (c) A schematic of the synthesis process for MoS_2/graphene composites. (d) TEM and high-resolution transmission electron microscopy of MoS_2/graphene. MoS_2@C-PNR (e) SEM image with a scale bar of 2 μm and (f) TEM image with a scale bar of 200 nm. (g) A schematic of the intercalation of solvated $[Mg(DME)_x]^{2+}$ in the MoS_2@C-PNR. Reproduced with permission from Liang *et al.*, Adv. Mater. **23**, 640 (2011). Copyright 2011 Wiley-VCH Verlag GmbH & Co.;[64] reproduced with permission from Liu *et al.*, J. Power Sources **340**, 104 (2017). Copyright 2017 Elsevier Ltd.;[81] reproduced with permission from Li *et al.*, Nat. Commun. **9**, 5115 (2018). Copyright 2018 Nature Publishing Group.[82]

ions from the electrolyte to the active surface of MoS_2. The larger spacing also facilitates the reversible Mg^{2+} ion insertion and extraction kinetics.[61] In a separate work using exfoliated graphene-like MoS_2/graphene hybrid as the cathode [Fig. 5(c)], a notable capacity (115.9 mA h/g) and good cyclic stability (82.5 mA h/g after 50 cycles) have been realized.[81] In this hybrid, the composite shows a three dimensional porous structure from exfoliated MoS_2 layers, and the graphene was inserted in the MoS_2, giving an expanded interlayer spacing of 0.98 nm, as shown in Fig. 5(d). The fast kinetics of Mg^{2+} ion intercalation were enabled by using solvated magnesium-ions ($[Mg(DME)_x]^{2+}$) in nanostructured MoS_2@C porous nanorods (MoS_2@C-PNR).[82] Representative SEM and TEM images of the MoS_2@C-PNR are shown in Figs. 5(e) and 5(f), respectively. The TEM shows an evenly distributed nanosheet array on the surface of the rod. Since the Mg^{2+} ion intercalation is limited by the low ion mobility because of the strong interaction between the Mg^{2+} ion and the host, the solvated $[Mg(DME)_3]^{2+}$ has a much larger volume per cation; thus, it will introduce a lower energy barrier compared to that of the Mg^{2+} ion, as shown in Fig. 5(g). It is worthy to notify that the concept involved in this study regarding adjusting the solvation of ions can be a general approach to deal with the intercalation kinetics, not only for Mg^{2+} ions but also for other cations. Similar to that mentioned in the Li- and Na-ion batteries, hybrid dual-ion energy storage is also of great interest in the Mg^{2+}/Li^{+} rechargeable batteries, combining the advantages of both Li- and Mg-electrochemistry.[1,83,84]

The aqueous zinc-ion battery has also received massive attention because it is of low cost, environmental friendly, and safe to operate.[85] With a high 1T-phase content of about 70%, the MoS_2 is able to introduce an excellent specific capacity and outstanding cycling stability. With information derived from *ex situ* x-ray diffraction (XRD), the reaction on the cathode side is $MoS_2 + xZn^{2+} + 2xe^{-} \rightarrow Zn_xMoS_2$ and that on the anode side is $xZn^{2+} + 2xe^{-} \rightarrow xZn$. Density functional theory (DFT) calculations reveal that the 1T-phase MoS_2 has a lower Zn^{2+} diffusion energy barrier compared to that of the 2H-phase MoS_2. The nanostructure engineering of the MoS_2 microsphere cathode has also been used in the aluminum-ion batteries.[60] In the discharge process, the Al^{3+} ion intercalate into the cathode through $MoS_2 + xAl^{3+} + 3xe^{-} \rightarrow Al_xMoS_2$, while the anode side reaction is $xAl + 7xAlCl_4^{-} \rightarrow 4xAl_2Cl_7^{-} + 3xe^{-}$. The discharge specific capacity is 253.6 mA h/g at a current density of 20 mA/g, and this system using the MoS_2 microsphere cathode also exhibits good cycling stability.

So far, various MoS_2-based electrode materials, including MoS_2 composites with different geometrical structures, have been reported in the literature for both lithium-ion and beyond lithium-ion batteries (Table I). The motivation for calcium-ion batteries was limited by the capability to plate and strip calcium at temperatures close to room temperature until the very recent work from Bruce *et al.*[89] Then, the solvation environment studies of Ca^{2+} ions have been performed using electrochemical and *in situ*/*operando* soft x-ray absorption spectroscopy (XAS).[40,90] As the research on calcium-ion

TABLE I. Electrochemical performance of numerous MoS_2-based electrode materials.

Materials	Capacity (mA h/g)	Current density (mA/g) or C	Cycles (%/retention)	Electrolyte	References
MoS_2/graphene	225	1000	200 (90)	PhMgCl and $AlCl_3$ and LiCl/THF all-phenyl-complex (APC)	1
MoS_2/C nanoflower	56	200	1000 (95)	Na_2SO_4 (aq)	86
MoS_2/polyaniline	159.9	1000	500 (98)	H_2SO_4 (aq)	87
MoS_2 nanotubes	260	50	30 (98)	KOH (aq)	6
MoS_2 nanobelt	520–540	1000	100 (98)	$NaClO_4$/propylene carbonate with 5% fluoroethylene carbonate	15
MoS_2	135	200	100 (~100)	$LiPF_6$/ethylene carbonate and diethyl carbonate (1:1)	17
MoS_2 nanosheet	1077	1000	400 (84)	$LiPF_6$/ethylene carbonate, dimethyl carbonate, ethyl methyl carbonate (1:1:1)	19
MoS_2/PEO/graphene	654	10 000	180 (65)	$LiPF_6$/ethylene methyl carbonate and ethylene carbonate (7:3)	26
MoS_2 hollow nanosphere	1100	500	100 (~100)	$LiPF_6$/ethylene carbonate, diethyl carbonate (1:1)	29
MoS_2 nanoflake/rGO	826	8C	600 (76)	LiTFSI, 2 wt. %$LiNO_3$/dioxolane, dimethoxyethane (1:1)	30
MoS_2/mesoporous C	1183	200	>500	$LiPF_6$/ethylene carbonate, dimethyl carbonate (1:1)	35
MoS_2/rGO microsphere	104.2	50	50 (71)	$AlCl_3$/PhMgCl electrolyte	57
MoS_2 microsphere	253.6	20	100 (26)	$AlCl_3$/1-ethyl-3-methylimidazolium chloride	60
MoS_2/C microsphere	213	50	20 (55)	$Mg_2Cl_3^+AlPh_2Cl_2^-$/THF	61
MoS_2/PEO	225	50	70 (66)	$NaCF_3SO_3$/diethyleneglycol dimethyl ether	62
Graphene-like MoS_2	170	71	60 (95)	$Mg(AlCl_3Bu)_2$/THF	64
MoS_2	85	50	100 (64)	$NaCF_3SO_3$/tetraethylene glycol dimethyl ether	73
Dual-phase MoS_2	670	100	200 (45)	$NaClO_4$/propylene carbonate with 5% fluoroethylene carbonate	76
Penne-like MoS_2/C	65	2C	200 (85)	$NaPF_6$/ethylene carbonate, ethyl methyl carbonate, dimethyl carbonate (1:1:1)	77
MoS_2/graphene	300	20	120 (97)	LiCl & all-phenyl-complex/THF	83
MoS_2/SiOC	92.9	200	100 (86.5)	$NaClO_4$/ethylene carbonate, dimethyl carbonate(1:1)	88

batteries is still in its infancy, not much experimental effort has been reported for the Ca^{2+} ion intercalation in MoS_2.

IV. *IN SITU*/*OPERANDO* CHARACTERIZATION METHODS

Another important aspect we would like to discuss separately is the characterization methods involved, especially those *in situ*/*operando* characterization methods used in the study of MoS_2 applications in the lithium-ion and beyond lithium-ion batteries, including *in situ*/*operando* XAS, XRD, and TEM. Such an *in situ*/*operando* setup makes it possible to probe the transient state species that cannot be performed under *ex situ* conditions.

Zhang *et al.* used *in situ*/*operando* XAS in the probing of MoS_2 anode intercalation and conversion reactions in lithium-ion cells, through which the irreversible conversion reaction of MoS_2 and conversion of Li_2S to S in the first charge process are confirmed.[17] As shown in Fig. 6(a), the *in situ*/*operando* sulfur K-edge XAS mapping shows no obvious change, and to visualize how the XAS spectra are developed, the intensity at 2471.5 eV is plotted as a function of specific capacity in Fig. 6(b). As summarized in Fig. 6(c), the intercalation of MoS_2 is reversible and associated with a phase transformation between 2H- and 1T-phases. The conversion reaction is not reversible and the discharge product Li_2S is converted to S in the first charge. The MoS_2 electrode also suppresses the shuttle effect in Li/S cells. The contrast between *in situ* and *ex situ* XAS measurements and valuable reaction dynamics information of MoS_2 are obtained.

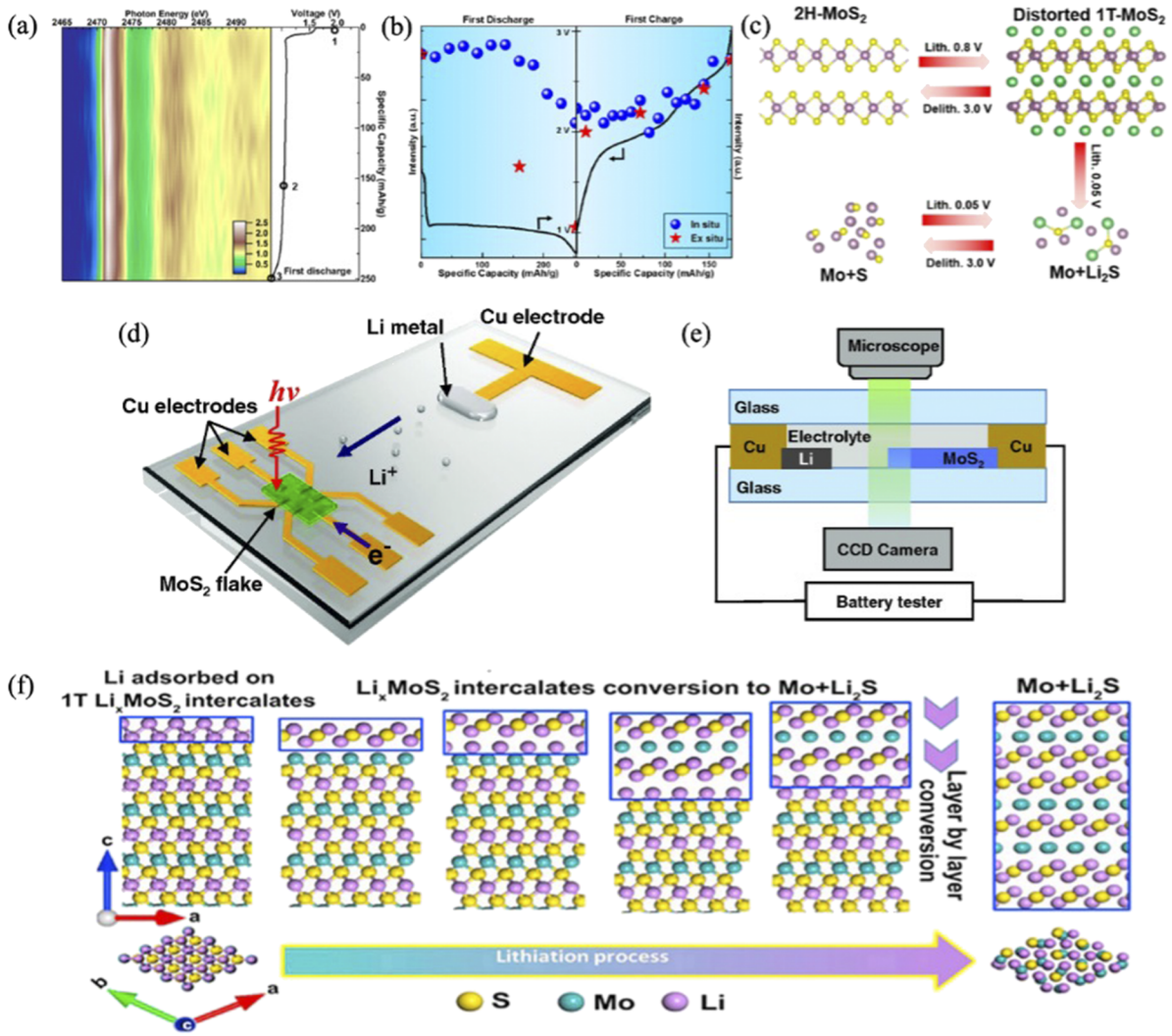

FIG. 6. (a) *In situ*/*operando* sulfur K-edge XAS mapping and the corresponding voltage profiles for the first discharge process. (b) Intensity evolution of MoS_2 as a function of specific capacity from *in situ* and *ex situ* XAS. (c) A schematic for the proposed MoS_2 electrode electrochemical reaction mechanism. A schematic for (d) the planar Li–MoS_2 microbattery and (e) the *in situ*/*operando* optical transmittance measurement of the MoS_2 lithiation. (f) A schematic of the proposed atomistic mechanism of layer-by-layer MoS_2 anode lithiation. Reproduced with permission from Zhang *et al.*, Nano Lett. **18**, 1466 (2018). Copyright 2018 American Chemical Society;[17] reproduced with permission from Li *et al.*, Energy Storage Mater. **9**, 188 (2017). Copyright 2017 Elsevier Ltd.;[32] reproduced with permission from Wan *et al.*, Adv. Energy Mater. **5**, 1401742 (2015). Copyright 2015 Wiley-VCH Verlag GmbH & Co.[91]

In another interesting work of a Li–MoS_2 microbattery, a planar battery geometry was employed to allow *in situ*/*operando* TEM probing during the electrochemical charge and discharge processes.[91] It was confirmed that in the first cycle of lithiation, the formation of a Mo conductive network in the Li_2S matrix results in boosted electrical conductivity and optical transmittance compared to the pristine MoS_2. A threefold capacity increase was realized after first cycle rapid lithiation compared to cells through a conventional constant-current discharge. In a separate work using *in situ* TEM, using a unique graphene@MoS_2 nanotube as the anode in the lithium-ion battery, a novel conversion reaction mechanism was confirmed.[32] Along the [001] direction, lithium ions incorporate to the Li_xMoS_2 surface, and the exchange of lithium with the sulfur atom is the reaction pathway for Li_2S formation. As shown in Fig. 6(f), the conversion reaction starts with 1T-Li_xMoS_2 and then intercalates into mixed metallic Mo and Li_2S domains. Eventually, the composites of Mo clusters are captured in the Li_2S matrix in a fully lithiated fashion. These examples for probing such transient processes at non-equilibrium states shown here can only be achieved with the *in situ*/*operando* experimental methods, which is critical for a fundamental understanding of the electrochemical reactions, offering additional insights.

V. SUMMARY AND PROSPECT

In summary, MoS_2 and composites containing MoS_2 have been proved to be promising candidates as electrode materials. The larger interlayer spacing makes them suitable for fast metallic ion diffusion, such as Na^+, Zn^{2+}, and Mg^{2+}. The natural abundance and the corresponding low cost of these beyond lithium-ion batteries demand large scale production of MoS_2. However, dual-ion batteries often rely on lithium-ion electrolytes, hindering their long-term development due to the limited lithium resources. Additionally, the 1T-phase MoS_2 nanosheets are intrinsically unstable, and the fabrication of MoS_2 with controlled interlayer spacing requires more novel approaches. The intercalation of the metallic ion will also induce transformation of its layered structures, such as interlayer spacing, which results in a significant irreversible loss of capacities in the first cycle; thus, additional methods to improve the stability are required. As a typical transition-metal chalcogenide, MoS_2 plays an important part not only in the lithium-ion and beyond lithium-ion energy storage devices, such as batteries and supercapacitors, but also with applications in catalysis studies, such as the hydrogen evolution reaction (HER) process. The approaches used in the MoS_2 nanostructure synthesis, including the MoS_2 of different geometries, e.g., microspheres, nanorods, and hollow-interior vesicles, and on different supporting substrates, e.g., graphene and rGO, are reported. Possible strategies to promote the energy storage properties of MoS_2 might include adjusting the solvation of ions to modify the intercalation kinetics, precisely controlling the MoS_2 phases since the 1T-phase MoS_2 has a lower diffusion energy barrier compared to that of the 2H-phase MoS_2, and regulating the mechanical strain meticulously to alter the adsorption energy and semiconducting gap of MoS_2. With a strong motivation for calcium-ion energy storage and the fact that not much experimental effort has been made for the Ca^{2+} ion intercalation in MoS_2, the strategies mentioned above should be exercised to develop better calcium-ion batteries. To further extend the scope, the beyond MoS_2 analog, such as TiS_2, VS_2, $MoSe_2$, and MoS_3, and other *in situ*/*operando* probing techniques, such as Raman, XPS, and resonant inelastic x-ray scattering (RIXS), should be considered to provide more insight into deciphering the reaction mechanism. From the perspective of application, the use of MoS_2 in the nitrogen reduction reaction (NRR) catalysis, the carbon dioxide reduction reaction (CO_2RR) may also benefit from the unique properties of MoS_2 and its analog.

ACKNOWLEDGMENTS

This work was supported by the Joint Center for Energy Storage Research, an Energy Innovation Hub funded by the U.S. Department of Energy. Soft x-ray spectroscopy experiments were carried out on the beamlines 5.3.1, 7.3.1, and 8.0.1 at the Advanced Light Source. This research used resources of the Advanced Light Source, a U.S. DOE Office of Science User Facility under Contract No. DE-AC02-05CH11231.

DATA AVAILABILITY

The data that support the findings of this study are available within the article.

REFERENCES

[1] C.-J. Hsu, C.-Y. Chou, C.-H. Yang, T.-C. Lee, and J.-K. Chang, Chem. Commun. **52**, 1701 (2016).
[2] T. Wang, S. Chen, H. Pang, H. Xue, and Y. Yu, Adv. Sci. **4**, 1600289 (2017).
[3] A. L. Santhosha, P. K. Nayak, K. Pollok, F. Langenhorst, and P. Adelhelm, J. Phys. Chem. C **123**, 012126 (2019).
[4] F. Yang, X. Feng, Y. Liu, L. C. Kao, P. Glans, W. Yang, and J. Guo, Energy Environ. Mater. **2**, 12172 (2021).
[5] R. R. Haering, J. A. R. Stiles, and K. Brandt, U.S. Patent **4**, 224, 390 (1980).
[6] J. Chen, N. Kuriyama, H. Yuan, H. T. Takeshita, and T. Sakai, J. Am. Chem. Soc. **123**, 011813 (2001).
[7] R. Tenne, Nat. Nanotechnol. **1**, 103 (2006).
[8] K. Chu, Y.-p. Liu, Y.-b. Li, Y.-l. Guo, and Y. Tian, ACS Appl. Mater. Interfaces **12**, 7081 (2020).
[9] K. Lv, C. Teng, M. Shi, Y. Yuan, Y. Zhu, J. Wang, Z. Kong, X. Lu, and Y. Zhu, Adv. Funct. Mater. **28**, 1802339 (2018).
[10] Y. Liu, M. Han, Q. Xiong, S. Zhang, C. Zhao, W. Gong, G. Wang, H. Zhang, and H. Zhao, Adv. Energy Mater. **9**, 1803935 (2019).
[11] S. Park, J. Park, H. Abroshan, L. Zhang, J. K. Kim, J. Zhang, J. Guo, S. Siahrostami, and X. Zheng, ACS Energy Lett. **3**, 2685 (2018).
[12] M. Chhowalla and G. A. J. Amaratunga, Nature **407**, 164 (2000).
[13] R. Tenne and M. Redlich, Chem. Soc. Rev. **39**, 1423 (2010).
[14] S. Yang, D. Li, T. Zhang, Z. Tao, and J. Chen, J. Phys. Chem. C **116**, 1307 (2012).
[15] Z. Zhang, S. Wu, J. Cheng, and W. Zhang, Energy Storage Mater. **15**, 65 (2018).
[16] L. Wang, Q. Zhang, J. Zhu, X. Duan, Z. Xu, Y. Liu, H. Yang, and B. Lu, Energy Storage Mater. **16**, 37 (2019).
[17] L. Zhang, D. Sun, J. Kang, J. Feng, H. A. Bechtel, L.-W. Wang, E. J. Cairns, and J. Guo, Nano Lett. **18**, 1466 (2018).
[18] B. G. Silbernagel, Solid State Commun. **17**, 361 (1975).
[19] Y. Teng, H. Zhao, Z. Zhang, Z. Li, Q. Xia, Y. Zhang, L. Zhao, X. Du, Z. Du, P. Lv, and K. Świerczek, ACS Nano **10**, 8526 (2016).
[20] Y.-X. Wang, S.-L. Chou, D. Wexler, H.-K. Liu, and S.-X. Dou, Chem. - Eur. J. **20**, 9607 (2014).
[21] X.-L. Li and Y.-D. Li, J. Phys. Chem. B **108**, 013893 (2004).
[22] F. Cheng, H. Wang, Z. Zhu, Y. Wang, T. Zhang, Z. Tao, and J. Chen, Energy Environ. Sci. **4**, 3668 (2011).
[23] M. R. Lukatskaya, B. Dunn, and Y. Gogotsi, Nat. Commun. **7**, 12647 (2016).
[24] T. Stephenson, Z. Li, B. Olsen, and D. Mitlin, Energy Environ. Sci. **7**, 209 (2014).
[25] H. Hwang, H. Kim, and J. Cho, Nano Lett. **11**, 4826 (2011).
[26] J. Xiao, X. Wang, X.-Q. Yang, S. Xun, G. Liu, P. K. Koech, J. Liu, and J. P. Lemmon, Adv. Funct. Mater. **21**, 2840 (2011).
[27] K. Chang and W. Chen, ACS Nano **5**, 4720 (2011).
[28] A. J. Jacobson, R. R. Chianelli, and M. S. Whittingham, J. Electrochem. Soc. **126**, 2277 (1979).
[29] Y. Wang, L. Yu, and X. W. D. Lou, Angew. Chem., Int. Ed. **55**, 7423 (2016).
[30] H. Lin, L. Yang, X. Jiang, G. Li, T. Zhang, Q. Yao, G. W. Zheng, and J. Y. Lee, Energy Environ. Sci. **10**, 1476 (2017).
[31] G. Zhao, Y. Cheng, P. Sun, W. Ma, S. Hao, X. Wang, X. Xu, Q. Xu, and M. Liu, Electrochim. Acta **331**, 135262 (2020).
[32] Y. Li, Z. Liu, X. Cheng, X. Liu, B. Zhang, D. Sun, R. Wang, and Y. Zhang, Energy Storage Mater. **9**, 188 (2017).
[33] S. N. Heo, Y. Ishiguro, R. Hayakawa, T. Chikyow, and Y. Wakayama, APL Mater. **4**, 030901 (2016).
[34] J. B. Cook, H.-S. Kim, Y. Yan, J. S. Ko, S. Robbennolt, B. Dunn, and S. H. Tolbert, Adv. Energy Mater. **6**, 1501937 (2016).
[35] H. Jiang, D. Ren, H. Wang, Y. Hu, S. Guo, H. Yuan, P. Hu, L. Zhang, and C. Li, Adv. Mater. **27**, 3687 (2015).
[36] A. S. Aricò, P. Bruce, B. Scrosati, J.-M. Tarascon, and W. Van Schalkwijk, Nat. Mater. **4**, 366 (2005).
[37] J. Xiao, D. Choi, L. Cosimbescu, P. Koech, J. Liu, and J. P. Lemmon, Chem. Mater. **22**, 4522 (2010).
[38] R. Kappera, D. Voiry, S. E. Yalcin, B. Branch, G. Gupta, A. D. Mohite, and M. Chhowalla, Nat. Mater. **13**, 1128 (2014).

[39]M. Acerce, D. Voiry, and M. Chhowalla, Nat. Nanotechnol. **10**, 313 (2015).
[40]F. Yang, Y.-S. Liu, X. Feng, K. Qian, L. C. Kao, Y. Ha, N. T. Hahn, T. J. Seguin, M. Tsige, W. Yang, K. R. Zavadil, K. A. Persson, and J. Guo, RSC Adv. **10**, 027315 (2020).
[41]V. Etacheri, R. Marom, R. Elazari, G. Salitra, and D. Aurbach, Energy Environ. Sci. **4**, 3243 (2011).
[42]B. Dunn, H. Kamath, and J.-M. Tarascon, Science **334**, 928 (2011).
[43]A. El Kharbachi, O. Zavorotynska, M. Latroche, F. Cuevas, V. Yartys, and M. Fichtner, J. Alloys Compd. **817**, 153261 (2020).
[44]C. Xu, B. Li, H. Du, and F. Kang, Angew. Chem., Int. Ed. **51**, 933 (2012).
[45]D. Aurbach, Z. Lu, A. Schechter, Y. Gofer, H. Gizbar, R. Turgeman, Y. Cohen, M. Moshkovich, and E. Levi, Nature **407**, 724 (2000).
[46]L. K. Tan, B. Liu, J. H. Teng, S. Guo, H. Y. Low, and K. P. Loh, Nanoscale **6**, 10584 (2014).
[47]M. Chhowalla, H. S. Shin, G. Eda, L.-J. Li, K. P. Loh, and H. Zhang, Nat. Chem. **5**, 263 (2013).
[48]Z. Zeng, T. Sun, J. Zhu, X. Huang, Z. Yin, G. Lu, Z. Fan, Q. Yan, H. H. Hng, and H. Zhang, Angew. Chem., Int. Ed. **51**, 9052 (2012).
[49]R. J. Smith, P. J. King, M. Lotya, C. Wirtz, U. Khan, S. De, A. O'Neill, G. S. Duesberg, J. C. Grunlan, G. Moriarty, J. Chen, J. Wang, A. I. Minett, V. Nicolosi, and J. N. Coleman, Adv. Mater. **23**, 3944 (2011).
[50]C. Zhi, Y. Bando, C. Tang, H. Kuwahara, and D. Golberg, Adv. Mater. **21**, 2889 (2009).
[51]Y. Hernandez, V. Nicolosi, M. Lotya, F. M. Blighe, Z. Sun, S. De, I. T. McGovern, B. Holland, M. Byrne, Y. K. Gun'Ko, J. J. Boland, P. Niraj, G. Duesberg, S. Krishnamurthy, R. Goodhue, J. Hutchison, V. Scardaci, A. C. Ferrari, and J. N. Coleman, Nat. Nanotechnol. **3**, 563 (2008).
[52]Y.-H. Lee, X.-Q. Zhang, W. Zhang, M.-T. Chang, C.-T. Lin, K.-D. Chang, Y.-C. Yu, J. T.-W. Wang, C.-S. Chang, L.-J. Li, and T.-W. Lin, Adv. Mater. **24**, 2320 (2012).
[53]K.-K. Liu, W. Zhang, Y.-H. Lee, Y.-C. Lin, M.-T. Chang, C.-Y. Su, C.-S. Chang, H. Li, Y. Shi, H. Zhang, C.-S. Lai, and L.-J. Li, Nano Lett. **12**, 1538 (2012).
[54]Y. Li, K. Chang, Z. Sun, E. Shangguan, H. Tang, B. Li, J. Sun, and Z. Chang, ACS Appl. Energy Mater. **3**, 998 (2020).
[55]Z. Zeng, Z. Yin, X. Huang, H. Li, Q. He, G. Lu, F. Boey, and H. Zhang, Angew. Chem., Int. Ed. **50**, 011093 (2011).
[56]W. Zhang, P. Zhang, Z. Su, and G. Wei, Nanoscale **7**, 018364 (2015).
[57]Y. Liu, L. Jiao, Q. Wu, Y. Zhao, K. Cao, H. Liu, Y. Wang, and H. Yuan, Nanoscale **5**, 9562 (2013).
[58]Y. Zhao, K. Zheng, and X. Sun, Joule **2**, 2583 (2018).
[59]S. M. George, Chem. Rev. **110**, 111 (2010).
[60]Z. Li, B. Niu, J. Liu, J. Li, and F. Kang, ACS Appl. Mater. Interfaces **10**, 9451 (2018).
[61]Y. Liu, L. Jiao, Q. Wu, J. Du, Y. Zhao, Y. Si, Y. Wang, and H. Yuan, J. Mater. Chem. A **1**, 5822 (2013).
[62]Y. Li, Y. Liang, F. C. Robles Hernandez, H. Deog Yoo, Q. An, and Y. Yao, Nano Energy **15**, 453 (2015).
[63]Y.-X. Wang, K. H. Seng, S.-L. Chou, J.-Z. Wang, Z. Guo, D. Wexler, H.-K. Liu, and S.-X. Dou, Chem. Commun. **50**, 10730 (2014).
[64]Y. Liang, R. Feng, S. Yang, H. Ma, J. Liang, and J. Chen, Adv. Mater. **23**, 640 (2011).
[65]Y. Yu, W. Li, Z. Yang, Y. Jiang, Z. Yu, and L. Gu, Carbon **78**, 455 (2014).
[66]K. Chang and W. Chen, Chem. Commun. **47**, 4252 (2011).
[67]C. Zhao, J. Kong, X. Yao, X. Tang, Y. Dong, S. L. Phua, and X. Lu, ACS Appl. Mater. Interfaces **6**, 6392 (2014).
[68]F. Xiong, Z. Cai, L. Qu, P. Zhang, Z. Yuan, O. K. Asare, W. Xu, C. Lin, and L. Mai, ACS Appl. Mater. Interfaces **7**, 12625 (2015).
[69]Q. Q. Xiong and Z. G. Ji, J. Alloys Compd. **673**, 215 (2016).
[70]R. Wang, S. Wang, D. Jin, Y. Zhang, Y. Cai, J. Ma, and L. Zhang, Energy Storage Mater. **9**, 195 (2017).
[71]L. David, R. Bhandavat, and G. Singh, ACS Nano **8**, 1759 (2014).
[72]F. Yang, D. Presto, Y. Pan, K. Liu, L. Zhou, S. Narayanan, Y. Zhu, Z. Peng, M. D. Soucek, M. Tsige, and M. D. Foster, Macromolecules **52**, 5074 (2019).
[73]J. Park, J.-S. Kim, J.-W. Park, T.-H. Nam, K.-W. Kim, J.-H. Ahn, G. Wang, and H.-J. Ahn, Electrochim. Acta **92**, 427 (2013).
[74]Q. Li, Z. Yao, J. Wu, S. Mitra, S. Hao, T. S. Sahu, Y. Li, C. Wolverton, and V. P. Dravid, Nano Energy **38**, 342 (2017).
[75]M. Hou, Y. Qiu, G. Yan, J. Wang, D. Zhan, X. Liu, J. Gao, and L. Lai, Nano Energy **62**, 299 (2019).
[76]J. Wu, J. Liu, J. Cui, S. Yao, M. Ihsan-Ul-Haq, N. Mubarak, E. Quattrocchi, F. Ciucci, and J.-K. Kim, J. Mater. Chem. A **8**, 2114 (2020).
[77]H. Zhu, F. Zhang, J. Li, and Y. Tang, Small **14**, 1703951 (2018).
[78]J. Hao, J. Zheng, F. Ling, Y. Chen, H. Jing, T. Zhou, L. Fang, and M. Zhou, Sci. Rep. **8**, 2079 (2018).
[79]F. Yang, Z. Jiang, Q. He, Z. Zhang, Y. Zhou, E. Karapetrova, M. D. Soucek, and M. D. Foster, ACS Appl. Mater. Interfaces **11**, 3555 (2019).
[80]L. C. Kao, X. Feng, Y. Ha, F. Yang, Y.-S. Liu, N. T. Hahn, J. MacDougall, W. Chao, W. Yang, K. R. Zavadil, and J. Guo, Surf. Sci. **702**, 121720 (2020).
[81]Y. Liu, L.-Z. Fan, and L. Jiao, J. Power Sources **340**, 104 (2017).
[82]Z. Li, X. Mu, Z. Zhao-Karger, T. Diemant, R. J. Behm, C. Kübel, and M. Fichtner, Nat. Commun. **9**, 5115 (2018).
[83]X. Fan, R. R. Gaddam, N. A. Kumar, and X. S. Zhao, Adv. Energy Mater. **7**, 1700317 (2017).
[84]Q. D. Truong, M. Kempaiah Devaraju, Y. Nakayasu, N. Tamura, Y. Sasaki, T. Tomai, and I. Honma, ACS Omega **2**, 2360 (2017).
[85]J. Liu, P. Xu, J. Liang, H. Liu, W. Peng, Y. Li, F. Zhang, and X. Fan, Chem. Eng. J. **389**, 124405 (2020).
[86]L.-Q. Fan, G.-J. Liu, C.-Y. Zhang, J.-H. Wu, and Y.-L. Wei, Int. J. Hydrogen Energy **40**, 010150 (2015).
[87]K.-J. Huang, L. Wang, Y.-J. Liu, H.-B. Wang, Y.-M. Liu, and L.-L. Wang, Electrochim. Acta **109**, 587 (2013).
[88]D. M. Soares and G. Singh, Nanotechnology **31**, 145403 (2020).
[89]D. Wang, X. Gao, Y. Chen, L. Jin, C. Kuss, and P. G. Bruce, Nat. Mater. **17**, 16 (2018).
[90]N. T. Hahn, J. Self, T. J. Seguin, D. M. Driscoll, M. A. Rodriguez, M. Balasubramanian, K. A. Persson, and K. R. Zavadil, J. Mater. Chem. A **8**, 7235 (2020).
[91]J. Wan, W. Bao, Y. Liu, J. Dai, F. Shen, L. Zhou, X. Cai, D. Urban, Y. Li, K. Jungjohann, M. S. Fuhrer, and L. Hu, Adv. Energy Mater. **5**, 1401742 (2015).